

# Micromagnetic simulations of first-order reversal curve (FORC) diagrams of framboidal greigite

Miguel A. Valdez-Grijalva,<sup>1,\*</sup> Lesleis Nagy,<sup>2</sup> Adrian R. Muxworthy<sup>1</sup>, Wyn Williams,<sup>3</sup> Andrew P. Roberts<sup>4</sup> and David Heslop<sup>4</sup>

<sup>1</sup>Department of Earth Science and Engineering, Imperial College London, London, SW72BP, UK. E-mail: [adrian.muxworthy@imperial.ac.uk](mailto:adrian.muxworthy@imperial.ac.uk)

<sup>2</sup>Geosciences Research Division, Scripps Institution of Oceanography, La Jolla, CA 92037, USA

<sup>3</sup>School of GeoSciences, University of Edinburgh, Edinburgh, EH93FE, UK

<sup>4</sup>Research School of Earth Sciences, Australian National University, Canberra, ACT 2601, Australia

Accepted 2020 May 12. Received 2020 May 5; in original form 2019 November 11

## SUMMARY

Greigite is a sensitive environmental indicator and occurs commonly in nature as magnetostatically interacting framboids. Until now only the magnetic response of isolated non-interacting greigite particles have been modelled micromagnetically. We present here hysteresis and first-order reversal curve (FORC) simulations for framboidal greigite ( $\text{Fe}_3\text{S}_4$ ), and compare results to those for isolated particles of a similar size. We demonstrate that these magnetostatic interactions alter significantly the framboid FORC response compared to isolated particles, which makes the magnetic response similar to that of much larger (multidomain) grains. We also demonstrate that framboidal signals plot in different regions of a FORC diagram, which facilitates differentiation between framboidal and isolated grain signals. Given that large greigite crystals are rarely observed in microscopy studies of natural samples, we suggest that identification of multidomain-like FORC signals in samples known to contain abundant greigite could be interpreted as evidence for framboidal greigite.

**Key words:** Environmental magnetism; Magnetic mineralogy and petrology; Rock and mineral magnetism.

## 1 INTRODUCTION

Greigite ( $\text{Fe}_3\text{S}_4$ ) is an authigenic ferrimagnetic mineral found in sediments (Roberts *et al.* 2011). It occurs in sulphate-reducing environments, and is an indicator that sulphate reduction has occurred (Roberts 2015). It is most commonly found in strongly interacting, close-packed clusters called framboids (Ariztegui & Dobson 1996; Roberts *et al.* 2011). It often co-occurs with authigenic pyrite ( $\text{FeS}_2$ ) framboids, where greigite framboids can grow before or after formation of an original generation of pyrite framboids (Rowan & Roberts 2006; Rowan *et al.* 2009).

The magnetic structure and stability of isolated greigite particles have been the subject of previous numerical studies (Muxworthy *et al.* 2013; Valdez-Grijalva *et al.* 2018a,b). These studies examined the effect of grain size, and identified the transition size for stable single-domain (SD) to single-vortex (SV) behaviour (~54 – 70 nm for equidimensional grains); at this threshold size the magnetic structure becomes non-uniform and the magnetic response

changes markedly. Numerical simulations have been performed for hysteresis and first-order reversal curve (FORC) properties of non-interacting SD and SV greigite dispersions (Valdez-Grijalva *et al.* 2018a; Valdez-Grijalva & Muxworthy 2019); however, the FORC properties of highly interacting greigite ensembles remain poorly understood. FORC diagrams are routinely used in environmental magnetism and palaeomagnetism to identify magnetic minerals (Roberts *et al.* 2014, 2018b). Muxworthy *et al.* (2013) made threshold transition calculations for linear chains of magnetostatically interacting greigite; however, such linear chains are only observed in magnetotactic bacteria. Inorganic greigite often occurs as framboidal clusters, so the findings of Muxworthy *et al.* (2013) cannot be applied directly to framboids. Given that natural framboidal structures are found commonly in greigite and magnetite (e.g. Rowan & Roberts 2006; Emmerton *et al.* 2013), there is a need to understand their magnetic hysteresis loops and FORC signatures. The magnetic moments of individual framboids are too small to measure, so we must develop numerical models to isolate their signals.

In this paper, we use a numerical micromagnetic finite element method (FEM) model to calculate the FORC response of framboidal greigite composed of highly interacting, close-packed 30 nm grains.

\* Now at Instituto Mexicano del Petróleo, Mexico City 07730, Mexico

At this size, isolated equidimensional grains can only occur in the SD state (Valdez-Grijalva *et al.* 2018a) and produce FORC signals characteristic of isolated SD grains with cubic magnetocrystalline anisotropy (Valdez-Grijalva *et al.* 2018a).

## 2 METHODS

### 2.1 The micromagnetic method

The numerical micromagnetic MERRILL FEM model (Ó Conbhuí *et al.* 2018) was used here to calculate FORC diagrams for strongly interacting greigite clusters. A ferromagnetic (*sensu lato*) material has a Gibbs free-energy  $E_G$ , which excluding the effects of thermal fluctuations and magnetostriction, can be written as (Brown 1963):

$$E_G = \int_{\Omega} (\phi_{\text{exchange}} + \phi_{\text{anisotropy}} + \phi_{\text{stray}} + \phi_{\text{external}}) d\Omega, \quad (1)$$

where  $\Omega$  is the ferromagnetic volume, so that integration is carried out over the ferromagnetic body. The  $\phi$  terms are described below. First, the exchange energy ( $\phi_{\text{exchange}}$ ) is given by:

$$\phi_{\text{exchange}} = A|\nabla \mathbf{m}|^2, \quad (2)$$

where  $\mathbf{m}$  is the reduced (unitary) magnetization vector and  $A$  is the exchange stiffness constant. The exchange energy is an expression that provides a continuum approximation of the energy density due to quantum-mechanical exchange forces between atomic spins (Landau & Lifshitz 1935).

For greigite, the magnetocrystalline anisotropy energy ( $\phi_{\text{anisotropy}}$ ) is dominated by the first term ( $K_1$ ) at room temperature (Winklhofer *et al.* 2014), and the anisotropy energy can be written in terms of the reduced magnetization:

$$\phi_{\text{anisotropy}} = K_1(m_x^2 m_y^2 + m_y^2 m_z^2 + m_z^2 m_x^2). \quad (3)$$

The magnetic Gibbs free-energy associated with the magnetostatic self-interaction ( $\phi_{\text{stray}}$ ) of the ferromagnetic body and the stray magnetic field ( $\mathbf{H}_{\text{stray}}$ ) it produces, is given by (Brown 1963):

$$\phi_{\text{stray}} = -\frac{\mu_0 M_S}{2} \mathbf{m} \cdot \mathbf{H}_{\text{stray}}, \quad (4)$$

where  $M_S$  is the saturation magnetization and  $\mu_0$  the permeability of free space. Finally, the energy ( $\phi_{\text{external}}$ ) due to the magnetostatic interaction of the ferromagnetic body and an external field ( $\mathbf{H}_{\text{external}}$ ) is:

$$\phi_{\text{external}} = -\mu_0 M_S \mathbf{m} \cdot \mathbf{H}_{\text{external}}. \quad (5)$$

Micromagnetic algorithms are used to find the equilibrium magnetization ( $\mathbf{m}$ ) by minimizing the Gibbs free-energy (Hubert & Schäfer 2000). Here, a modified gradient-descent method is used (Ó Conbhuí *et al.* 2018). The non-local problem of calculating the stray field is handled via a hybrid finite-element/boundary-element formulation (Fredkin & Koehler 1990). Numerical solutions require a discretization of the spatial domain into a grid or mesh with a finite number of points on which numerical solutions are calculated. A FEM is used in MERRILL where 3-D space is decomposed into tetrahedral pieces called finite elements with the vertices of these elements called the nodes. On each mesh node, a unit vector is initially defined to create an initial guess; the micromagnetic algorithm then attempts to minimize the magnetic Gibbs free-energy by varying the orientation of each vector while ensuring that they remain unitary.

To model greigite at room temperature, we use the same parameters as outlined in Valdez-Grijalva *et al.* (2018a,b), which

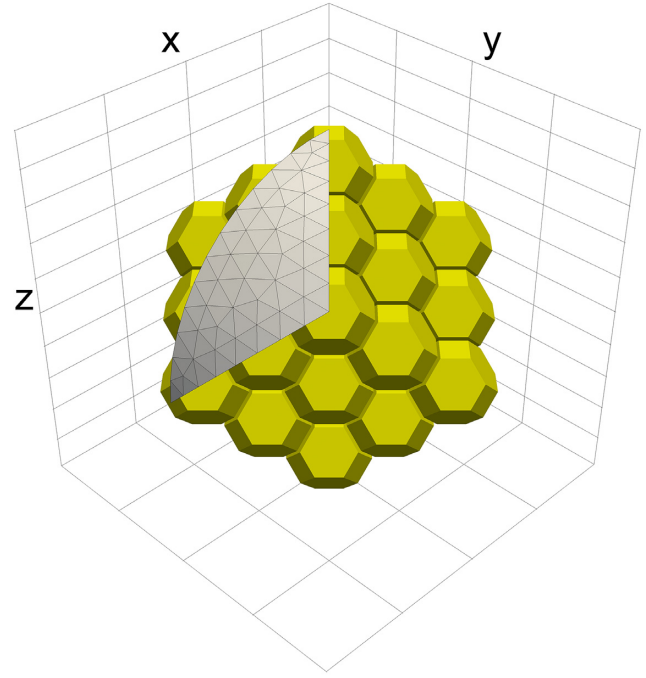


**Figure 1.** Framboidal mesh and field orientations. Field orientations are obtained from a triangular mesh over the spherical triangle delimited by  $(1, 0, 0)$ ,  $(1/\sqrt{3}, 1/\sqrt{3}, 1/\sqrt{3})$ ,  $(0, 0, 1)$ . Given the cluster symmetry, this region contains all field orientations of interest. The framboid contains 65 truncated octahedral particles each with size  $d = 30$  nm. The small gap between particles is  $\sim 2$  nm. The grey mesh contains an illustration of the angles over which the 85 directions were calculated.

are: (1)  $M_S = 2.7 \times 10^5$  A m<sup>-1</sup> (Li *et al.* 2014), (2)  $A = 2 \times 10^{-12}$  J m<sup>-1</sup> (Chang *et al.* 2008) and (3)  $K_1 = -1.7 \times 10^4$  J m<sup>-3</sup> (Winklhofer *et al.* 2014). To model nonuniform structures it is sufficient that the spatial discretisation in the model is always smaller than the exchange length  $l_{\text{exch}} = \sqrt{2A/\mu_0 M_S^2}$  (Hubert & Schäfer 2000), which for greigite is  $l_{\text{exch}} \approx 6.6$  nm; a maximum element size of 5 nm was chosen here for all meshes.

Truncated-octahedral particles were chosen for the model geometry because authigenic greigite particles typically have such morphology (Snowball 1997; Roberts *et al.* 2011), and truncated-octahedral solids can efficiently tessellate 3-D space and, thus, produce the close-packed geometries observed in framboidal greigite (Fig. 1). Touching grains are theoretically problematic to model because intergrain exchange coupling is not well understood. Here, a vanishing exchange coupling is assumed. Framboidal geometries with small gaps ( $\sim 2$  nm) between particles were used, so the only interparticle interaction is magnetostatic. Particles within a framboid are assigned the same magnetocrystalline anisotropy orientation. In nature, framboids exist where constituent particles are aligned and also randomly aligned (Ohfuji *et al.* 2006).

In this study we consider the behaviour of individual framboids and ensembles of randomly oriented framboids. In an ensemble of randomly oriented particles/framboids, there are equal probabilities of finding particles with any orientation within an area element of the unit sphere. To simulate a randomly oriented dispersion of identical particles efficiently, it is necessary to model a number of applied field directions (equivalently, particle orientations with respect to the applied field) each of which is representative of a given area on the unit sphere. Given the cubic symmetry of the modelled framboidal cluster geometries (Fig. 1) it is sufficient to

simulate the effects of field orientations on the spherical triangle delimited by  $(1, 0, 0)$ ,  $(1/\sqrt{3}, 1/\sqrt{3}, 1/\sqrt{3})$ ,  $(0, 0, 1)$  (Valdez-Grijalva *et al.* 2018a; Valdez-Grijalva & Muxworthy 2019). Then, the spherical triangle is subdivided into roughly equal triangular subunits to obtain 85 triangular cells; this was found to accurately represent a random distribution over the whole sphere. Each cell represents a field orientation, with the coordinates of the centre of the cell used as the field direction. The weighted average (cell area)/ $4\pi$ ) uses the cell area as the weight for each field direction, and is used to calculate the response for each field orientation as an approximation to the total magnetic response of a framboid ensemble.

## 2.2 The FORC model

FORCs are a set of partial hysteresis curves obtained from magnetization states on the upper branch of the hysteresis loop for different field values  $B_a$  (Pike *et al.* 1999; Roberts *et al.* 2000). For a given  $B_a$  and  $M(B_a)$ , the field  $B = B_b$  is increased to positive saturation to trace a magnetization curve. This procedure is repeated for a number of  $B_a$  values to create a magnetization function with two variables  $M = M(B_a, B_b)$  for  $B_b \geq B_a$ . The FORC distribution  $\rho$  is then defined as (Pike *et al.* 1999; Roberts *et al.* 2000):

$$\rho = -\frac{\mu_0^2}{2} \frac{\partial^2 M}{\partial B_a \partial B_b}. \quad (6)$$

Contour plots of the FORC distribution are called FORC diagrams and have been used extensively as a proxy for the magnetic domain state and magnetic reversal behaviour of a variety of systems (e.g. Pike *et al.* 2001; Dumas *et al.* 2007; Zhao *et al.* 2017). The standard method to calculate FORC distributions (eq. 6) is to perform least-squares fitting of a second-degree polynomial surface  $M(B_a, B_b) = a_0 + a_1 B_a + a_2 B_b + a_3 B_a B_b + a_4 B_a^2 + a_5 B_b^2 + e$ , where  $e$  is a collection of error terms, on a subgrid of the magnetization function  $M(B_a, B_b)$  including  $(2 \times \text{SF} + 1)^2$  points in the vicinity of  $(B_a, B_b)$  as determined by the smoothing factor SF (Pike *et al.* 1999); if the magnetisation is approximated in this manner, calculation of eq. (6) yields  $\rho = -\mu_0^2 a_3/2$ . Other fitting algorithms have also been developed (e.g. Harrison & Feinberg 2008; Egli 2013; Egli & Winklhofer 2014), but here we adopt the original approach of Pike *et al.* (1999). We use SF = 2 in all figures.

FORC simulations are computationally intensive, so we have developed an approach that reduces the number of calculations required. For each field orientation, the upper hysteresis loop branch is calculated. Most of the curve is traced by the sum of reversible magnetization motions in each particle in the framboid. Through analysis of  $>500$  reversible/irreversible processes during hysteresis we developed a set of criteria to identify an irreversible process, which meant that FORCs need only be calculated for  $B_a$  field values for which at least one particle undergoes an irreversible rotation (switching, Valdez-Grijalva *et al.* 2018a; Valdez-Grijalva & Muxworthy 2019). These criteria were: (a) rotation of the magnetization by  $5^\circ$  or more from one step to the next and (b) a normalized net magnetization drop  $>0.2$  from one step to the next. A field of  $B_{\text{max}} = 250$  mT was found to saturate the structure. An external field step of 2 mT was used for all calculations. Thus, for each field orientation we calculate 251 FORCs to obtain the FORC signal of a single cluster orientation. The simulations were performed on the Imperial College Research Computing Service HPC cluster and the Terrawulf III cluster at the Australian National University.

## 3 RESULTS

### 3.1 Simulated hysteresis and FORC responses of individual framboids

In our models, individual grains within a framboid all have the same orientation with respect to each other (Fig. 1), that is, all 30 nm particles have the same orientation. Therefore, the FORC response depends on the field orientation with respect to the framboid.

We consider first the case where the field is close to the framboid easy axis  $\langle 111 \rangle$ . During hysteresis the magnetic structure of this framboid is saturated at low fields  $\sim 50$  mT, and all of the 30 nm particles in the framboid remain in a SD state (Fig. 2a). Local interaction fields cause the outer particles in the framboid to rotate coherently to minimise stray fields as the applied field decreases. The remanent state is a double magnetic supervortex with a low remanence  $\sim 0.1 M_S$  that is due to the effective magnetic flux-closure (Harrison *et al.* 2002) (Fig. 3; see Supplementary Materials for animations of these images). The FORC diagram for this easy axis orientation has a positive peak at  $B_c \approx 80$  mT,  $\sim 5$  mT above the  $B_u = 0$  axis. A negative response of comparable magnitude is situated below and to the left of the distribution peak. The positive peak response corresponds to the large upward jumps experienced by the reversal curve starting at the switching field  $B_a \approx -80$  mT as it approaches positive saturation (Fig. 2a). The negative response is caused by irreversible switching of individual particles in the framboid on FORCs with higher  $B_a$  values at  $B_b \approx 75$  mT. This combination of negative and positive peaks has been reported previously for vortex systems (Pike & Fernandez 1999; Carvallo *et al.* 2003; Valdez-Grijalva *et al.* 2018a). FORC diagrams for these highly artificial numerical systems have many peaks and troughs compared to measurements on natural samples due to the discrete responses of individual grains to local interaction fields. However, a large positive response close to the  $B_c = 0$  axis, that is,  $B_c < 20$  mT, is important because it was found for all field orientations.

When the field is applied along the hard axis  $\langle 100 \rangle$ , the hysteresis and FORC responses contrast to that of the easy-axis case (Fig. 2). The hysteresis main branches are more rounded, and switching occurs via reversible rotations, that is, no discrete jumps during the rotation, with the first irreversible switching occurring at  $\sim 150$  mT on reducing the field from saturation (Fig. 2c). This gives rise to much smaller jumps than observed for the easy-axis aligned model (Fig. 2a). The main peaks in the FORC diagram (Fig. 2d) are closer to the  $B_c = 0$  axis, that is,  $B_c < 20$  mT, than in Fig. 2b.

### 3.2 Simulated hysteresis and FORC response of framboidal clusters

Averaging the response for all 85 field orientations results in a set of partial hysteresis curves, i.e., the raw FORCs, which are smooth and lack any discrete jumps (Fig. 4a). The saturation remanence ( $M_{RS}$ ) normalized by  $M_S$  for the framboid ensemble is  $M_{RS}/M_S \approx 0.1$  and the coercive force is  $B_c \approx 5$  mT; this contrasts sharply with the remanence and coercive force of a non-interacting ensemble of isolated SD greigite particles of the same size that have  $M_{RS}/M_S \approx 0.86$  and  $B_c \approx 24$  mT (Valdez-Grijalva *et al.* 2018a). Lower values for framboids are due to magnetostatic interactions among the constituent particles, and formation of supervortex states (Fig. 3). The minimum field required to saturate the magnetization, that is, to make it uniform in a given direction is 150 mT.

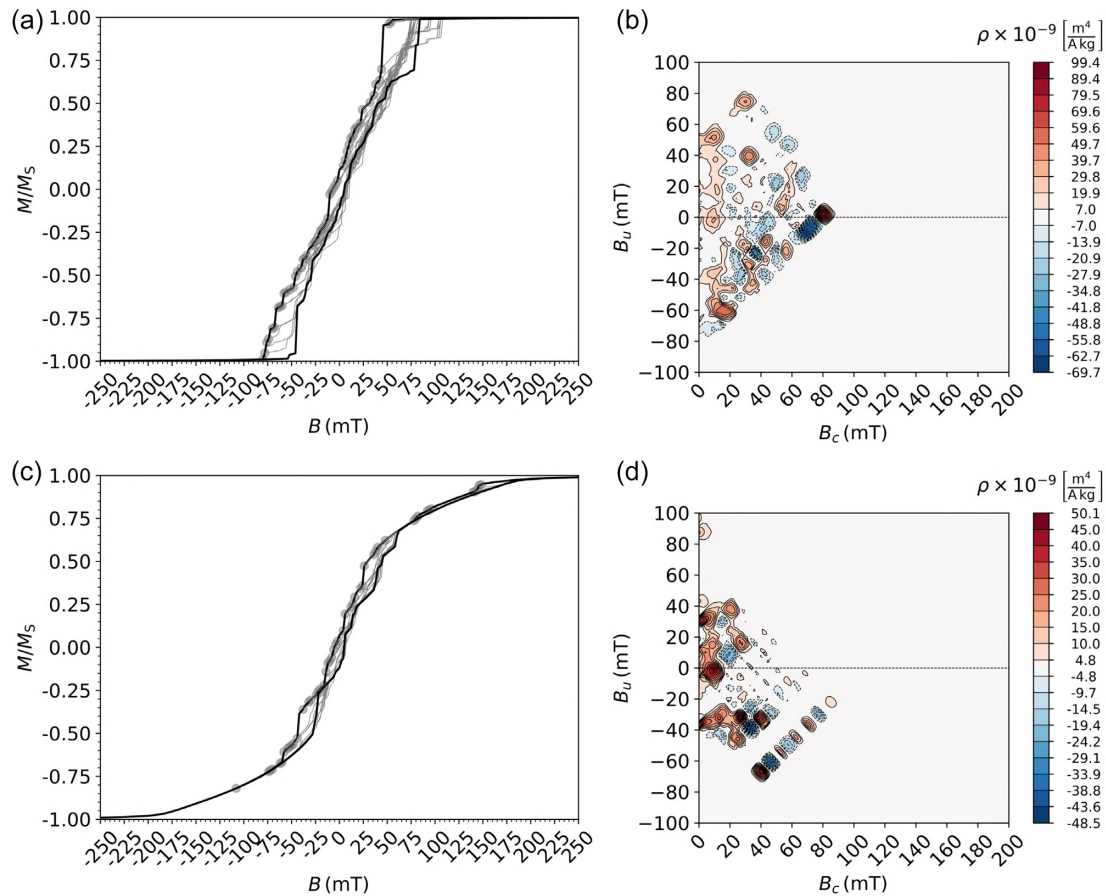


**Figure 2.** FORCs and FORC diagrams for framboidal greigite clusters with 30 nm crystallites for fields along an (a, b) easy and a (c, d) hard axis. When the field is aligned close to an easy axis, there is a peak FORC response on the  $B_u = 0$  axis at  $B_c \approx 80$  mT (b). For fields close to the hard axis, the FORC response has a peak at  $B_c \approx 10$  mT (d). SF = 2 for both FORC diagrams.

The main feature of the simulated FORC diagram for an ensemble of framboidal clusters (Fig. 4b) is a large response centred roughly at  $B_c = 10$  mT and  $B_u = 0$  mT and two lobes roughly at  $B_c = 10$  mT and  $B_u = \pm 40$  mT. These features are part of a larger, continuous signal, as highlighted by the box in Fig. 4(b). Negative and smaller positive responses lie in a region to the right of this rectangle; however, these features are only  $\sim 20$  per cent of the magnitude of the peak response at maximum, and at most are  $< 10$  per cent of the peak FORC distribution value.

### 3.3 Hysteresis of larger framboids

An attempt was made to simulate FORC diagrams for framboids consisting of assemblages of greigite particles, which when isolated are in the SV state, that is,  $> 70$  nm. Computational memory and calculation time constraints meant that the FORC response of these framboids with larger particles could not be simulated. Instead, we performed hysteresis simulations of framboids composed of fifteen larger particles ( $d = 76$  nm) (compared to 65 particles in Section 3.2), which are in the SV state when isolated (Valdez-Grijalva *et al.* 2018a, b). We modelled only 40 field orientations. When a saturating field of 250 mT is applied close to the easy axis, the magnetic structure remains nearly uniform until the field is reduced to  $\sim 50$  mT (Fig. 5; see Supplementary Materials for an animation of these images). As the field is further decreased,

outer particles in the framboid nucleate hard-aligned single-vortices (Fig. 5a). The remanent state (Fig. 5b) has a supervortex structure in which most particles are individually in a two-domain state with clearly defined domain walls (Fig. 5b, green). This state is similar to the easy-aligned SV state exhibited by large  $> 200$  nm particles (Valdez-Grijalva *et al.* 2018b) with six easy aligned domains curling around the vortex core. In this supervortex structure, outer particles are in a two-domain state and the six easy aligned magnetic domains span multiple particles. Non-interacting 76 nm particles nucleate vortices in the remanence state (Valdez-Grijalva *et al.* 2018a); however, for this field orientation, the innermost particle in the cluster always remains in a SD state due to internal magnetostatic interactions (Fig. 5b, grey line). This is likely true for larger framboids because relatively more grains will be inside the framboid and the number of grains at the edge of the framboid that experience lower inter-grain magnetostatic interaction fields will be reduced. Grains inside the framboid are more likely to be in a SD state. This suggests that for larger framboids composed of many larger particles, the FORC signal could be similar to that of framboids composed of SD particles (Section 3.2).

## 4 DISCUSSION

The FORC response of an anisotropic framboidal cluster depends strongly on the orientation of the framboid relative to the applied

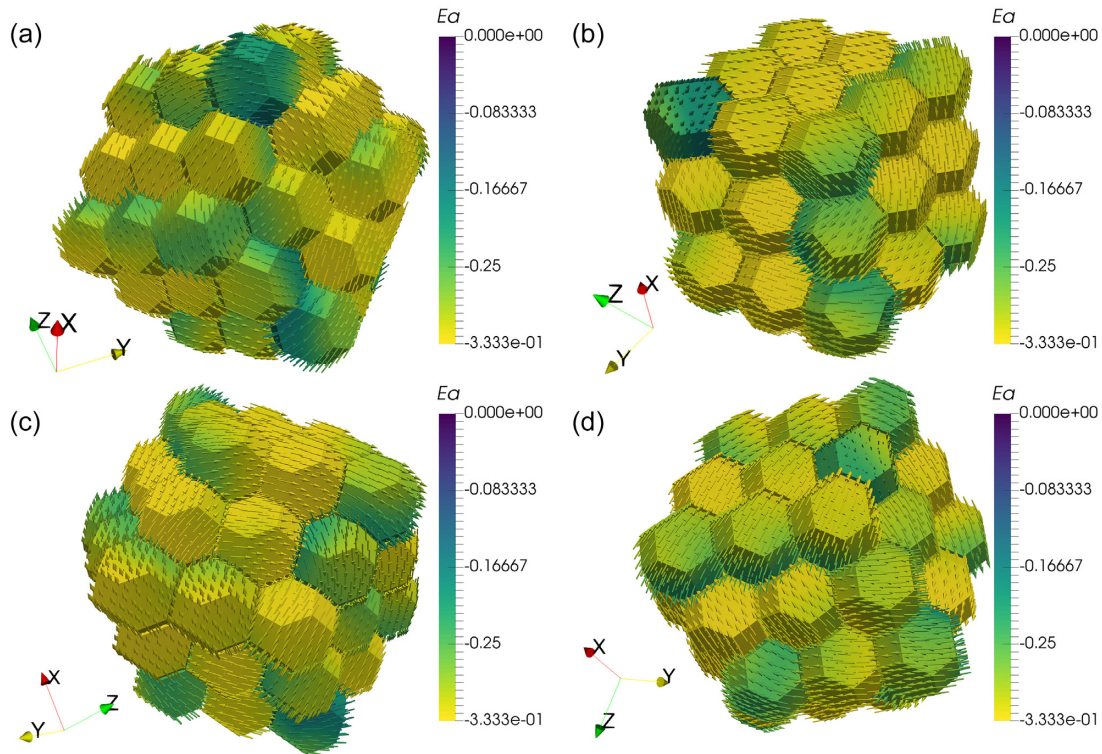


**Figure 3.** Various framboid saturation-remnance magnetic states (supervortex states). For fields (a) close to an easy axis, (b) close to a hard axis, (c) close to a saddle point and (d) close to an intermediate direction between the easy, hard, and saddle point directions. There are 85 applied field orientations in total. The net magnetic moment of the total ensemble is  $\sim 12^\circ$  from the applied field. See supplementary material for short animations of these images.

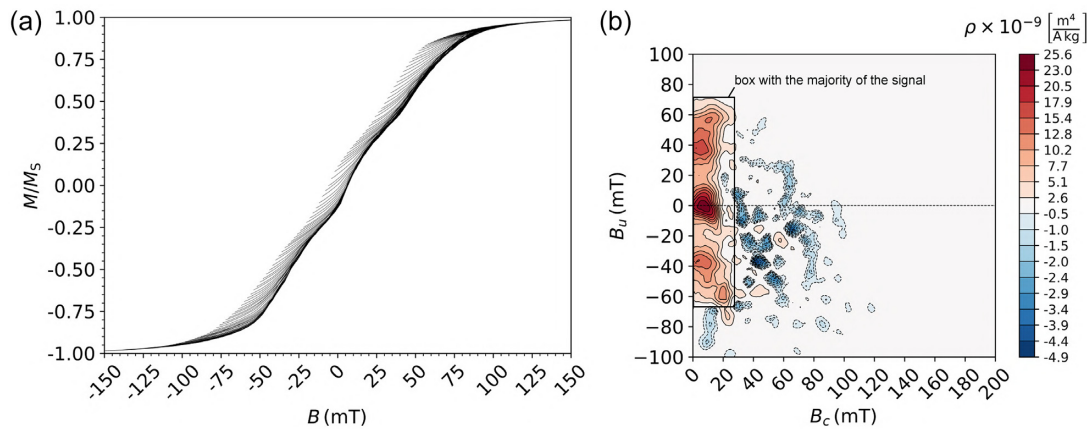


**Figure 4.** Simulated FORCs for the greigite framboid dispersion. The framboids consist of 65 particles aligned identically and with equal size  $d = 30$  nm. (a) When averaged over the 85 field directions, the raw hysteresis/FORCs are smooth and (b) the FORC response is MD-like ( $SF = 2$ ). The box discussed in the text is highlighted in (b).

field. When the field is aligned with an easy axis ( $\langle 111 \rangle$ ) the peak signal lies on the  $B_u = 0$  axis at  $B_c \approx 80$  mT (Fig. 2b). When the FORC response is averaged over 85 applied field directions, the main feature in the FORC diagrams is a vertical, almost-continuous feature in the box defined by  $B_c \approx 0$  to 10 mT and  $B_u \approx -60$  mT to 60 mT (Fig. 4b).

Remanence states for all simulated framboid configurations are supervortex states (Figs 3 and 5). Supervortex states form to create flux-closure, akin to closure domains in multidomain systems.

These super-vortex states reduce the net magnetisation of each framboid, which means that interframboidal interactions are likely weak even when multiple framboids occur relatively close to each other as is often observed in nature (e.g. Roberts 2015). The saturation-remnance net magnetic moment of the simulated framboid ensemble deviates from the applied field direction by  $\sim 12^\circ$ ; this deviation is due to a combination of inter-grain magnetostatic interaction fields and magnetocrystalline anisotropy. This observation raises the possibility that framboidal greigite may not carry

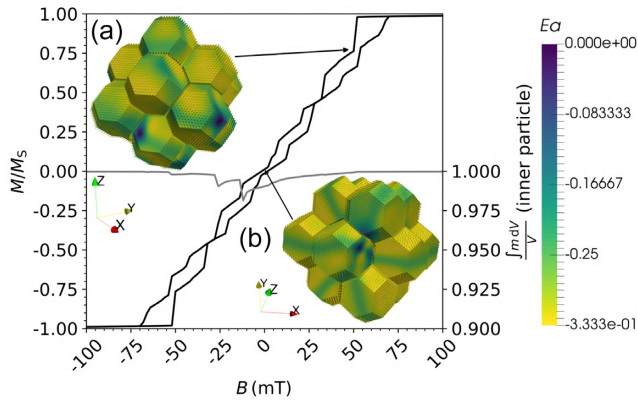


**Figure 5.** Hysteresis loop for a framboid with 76 nm particles for a field aligned close to the easy-anisotropy axis. Due to numerical limitations, the framboid consists of only 15 crystallites. On reducing the field from saturation, (a) the magnetization remains saturated to  $\sim 50$  mT when a few particles nucleate vortices. (b) The remanent state is a super-vortex structure with most particles in a two-domain-like state. Domain walls are visible as thin, green regions. The grey line is the reduced magnetization of the middle particle within the framboid during reduction of the external field. The right-hand vertical axis is the reduced magnetisation; the closer the magnetisation is to one, the greater SD the magnetic structure during hysteresis. Values below  $\sim 0.8$  (on the right-hand axis) start to display non-SD-like structures. The middle particle switches direction between  $\sim -15$  and  $-25$  mT.

meaningful palaeomagnetic directions; however, given the low number of particles within framboids (65) and the low number of directions (85) used to determine the net magnetisation direction, further numerical framboidal studies are needed to resolve this issue.

For framboids composed of 30 nm particles, that is, particles that are in the SD state when isolated, all individual particles in a framboid are SD. The remanence state for framboids consisting of 76 nm particles consists of SD structures for innermost particles, whilst outer particles contribute to what appear to be domain wall-like structures (Fig. 5). Intergrain and internal magnetostatic interaction fields within the framboid with 76 nm particles appear to give rise to similar net structures to those found for  $\sim 200$  nm isolated greigite grains, where domain-wall structures begin to initiate (Valdez-Grijalva *et al.* 2018b).

The FORC response of a simulated clustered greigite ensemble (Fig. 4) contrasts with that of isolated SD and SV grains (Valdez-Grijalva *et al.* 2018a). Isolated SD greigite particles produce FORC signals with a characteristic boomerang shape, strong  $B_u = 0$  contributions and a tilted negative ridge, while SV grains produce a more complex pattern. For isolated SD and SV grains, the FORC response is dominated by irreversible switching, which is evident in raw hysteresis/FORC data. In contrast, for framboidal greigite, the ensemble raw data are smooth (Fig. 4a), that is, there are no preferred coercivities at which irreversible jumps occur in all or many field directions.

The simulated FORC diagram for framboidal greigite (Fig. 4b) is similar to that for MD particles (Pike *et al.* 2001; Muxworthy & Dunlop 2002). These similarities occur because greigite framboids have especially MD-like behaviour because there are no exchange interactions between individual constituent grains. Exchange interactions tend to hinder MD behavior which is characterized by optimal flux closure.

#### 4.1 Combining the FORC responses of framboids and isolated grains

If we compare the FORC response of framboid clusters made up of 30 nm grains to that of an ensemble of isolated 30 nm grains determined by Valdez-Grijalva *et al.* (2018a), we find that the peak value of the FORC distribution is substantially smaller:  $25.6 \times 10^{-9} \text{ m}^4 \text{ A}^{-1} \text{ kg}^{-1}$  compared to  $531.6 \times 10^{-9} \text{ m}^4 \text{ A}^{-1} \text{ kg}^{-1}$ , respectively. For an assemblage of 80 nm SV particles the peak value of the FORC distribution is  $387.9 \times 10^{-9} \text{ m}^4 \text{ A}^{-1} \text{ kg}^{-1}$  (Valdez-Grijalva *et al.* 2018a). Therefore, for nearly equal mixtures of framboids and isolated particles, the latter will dominate the FORC response. We demonstrate this dominance in Fig. 6, where we combine FORC model results from Valdez-Grijalva *et al.* (2018a) for isolated particles with our framboid results. We consider two scenarios: (1) the FORC response of framboids with that of isolated greigite particles in the SD size range 30–48 nm (Fig. 6a) and (2) framboids with isolated particles in the SV grain size range 70–80 nm (Fig. 6b); in both cases the framboidal contribution has been enhanced by adding five times as much by mass compared to the isolated particles. The size distribution of isolated particles is constant. In the first case, isolated particles have SD behaviour, and in the second case only SV behaviour (Valdez-Grijalva *et al.* 2018a). The mixture of framboidal and isolated SD greigite particles (Fig. 6a) is dominated by the isolated SD signal; however, the framboidal signal close to the  $B_c = 0$  axis is represented clearly in the FORC space, although the less intense framboidal FORC features (Fig. 4b) are hidden by the SD signal. When the signals of isolated SV particles and framboids are combined (Fig. 6b), the FORC response is again dominated by the isolated particles. The framboidal and SV responses mostly overlap and plot within the same area, that is, close to the  $B_u$  axis; however, the framboidal signal is more dominant in the positive  $B_u$  region of the diagram.

Based on visual comparisons, simulated FORC responses for mixtures of framboidal and isolated SD grains (Fig. 6a) are similar to those of framboidal-greigite-rich samples from Taiwan obtained by Chou *et al.* (2012), but are less similar to the FORC response typically identified for greigite (e.g. Rowan & Roberts 2006; Roberts *et al.* 2018b). The samples from Chou *et al.* (2012) might be atypical because they were heated during a fault slip event, whereas most other greigite-rich samples have not been subjected to heat. Therefore, it would appear that the FORC diagrams reported by Rowan & Roberts (2006) and many others represent non-framboidal interacting particle systems; however, electron microscopy observations reveal the presence of framboidal greigite (e.g. Rowan & Roberts 2006; Roberts *et al.* 2011). This apparent disconnect between observed and simulated FORC responses might be explained by several mechanisms: (1) alteration of greigite to pyrite on crystal surfaces (and *vice versa*) as observed by Ebert *et al.* (2018). If crystal surfaces are altered to a non-magnetic phase, for example, pyrite, this would increase the effective distance between magnetic particles and reduce magnetic interactions to give rise to reduced vertical spreading in FORC diagrams (Muxworthy *et al.* 2004), but would produce high coercivities similar to those observed for isolated particles. This means that FORC diagrams could potentially hold information about the degree of pyritisation of a greigite-rich sample. (2) In nature, framboids are rarely as tightly packed as those modelled, that is, particle sizes and orientations are less uniform which would result in relatively greater particle separation within framboids (Ohfuji & Rickard 2005; Rickard 2019). Hüsing *et al.* (2009) demonstrated that greigite can occur as framboids, non-framboidal masses, and as isolated particles in the same

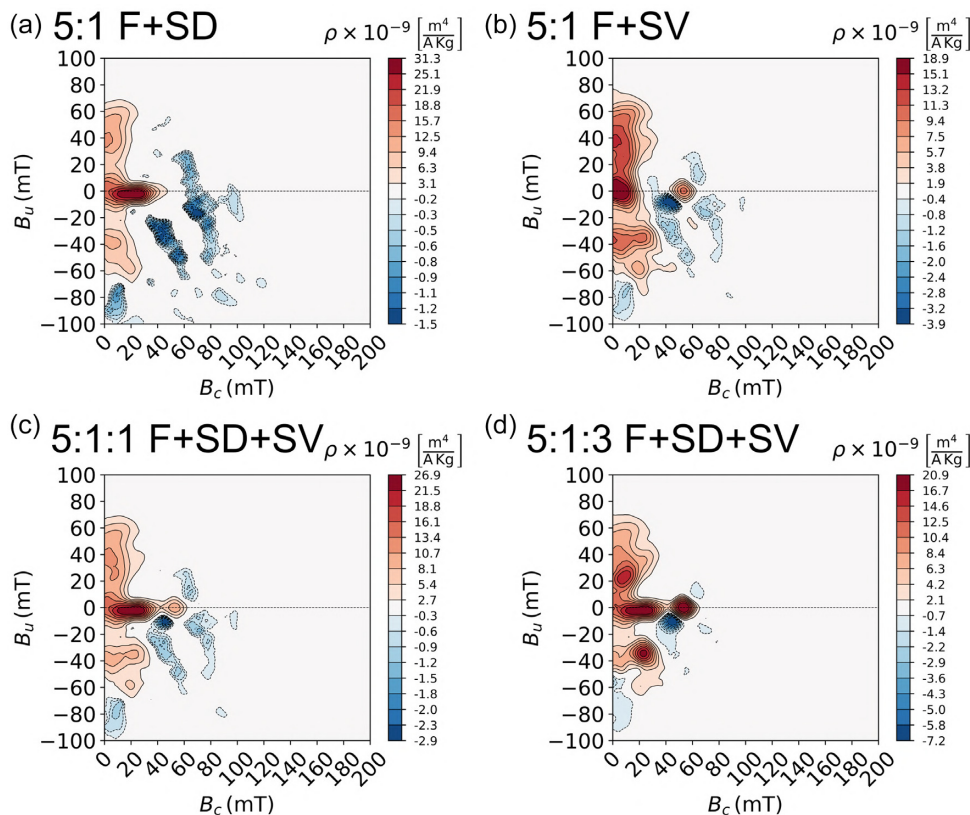


**Figure 6.** Simulated FORC diagrams for dispersions of frambooids mixed with isolated particles. In (a) isolated particles are all in the SD size range (30–48 nm) and in (b) SV particles are modelled in the size range 70–80 nm. The frambooidal (F), SD and SV simulations are mixed in varying proportions: (a) 5:1 F:SD, (b) 5:1 F:SV, (c) 5:1:1 F:SD:SV and (d) 5:1:3 F:SD:SV.  $SF = 2$  in all FORC diagrams. The signal is dominated by the non-interacting particles because the frambooidal signal is weaker per unit mass. The frambooidal signal is still visible because it occupies regions that the isolated particles do not. Solutions for isolated particles are taken from Valdez-Grijalva *et al.* (2018a).

system. Such systems will give rise to higher coercivity FORC diagrams. (3) Many magnetic studies that are combined with electron microscopy might have focused on identifying the presence of frambooids, which may not be representative of the bulk magnetic response.

#### 4.2 Frambooidal hysteresis behaviour and the ‘Day’ plot

The ‘Day plot’ (Day *et al.* 1977) is a graph of  $M_{RS}/M_S$  versus  $B_{CR}/B_C$ , where  $B_{CR}$  is the coercivity of remanence. We determined  $B_{CR}$  from the FORC simulations, therefore we estimated it from FORCs that crossed the near the origin, rather than from a series of minor hysteresis loops, which is the standard method of calculating  $B_{CR}$ . Despite the many factors that can contribute to ambiguity in interpreting data distributions in the Day diagram (Roberts *et al.* 2018a), hysteresis parameters are sensitive to domain state variations for particles of a single size, which is one case in which data distributions on the Day plot can be interpreted more clearly (Fig. 7). We also include in Fig. 7 results from Valdez-Grijalva *et al.* (2018a) for isolated particles, and for the mixtures described in Section 4.1. All calculations are for randomly oriented particle distributions. Data for isolated particles with a defined grain size follow a well-documented trend in the Day plot, as particles transition from the SD to the SV state (Muxworthy *et al.* 2003). The frambooidal signal and that of mixtures of frambooidal and isolated

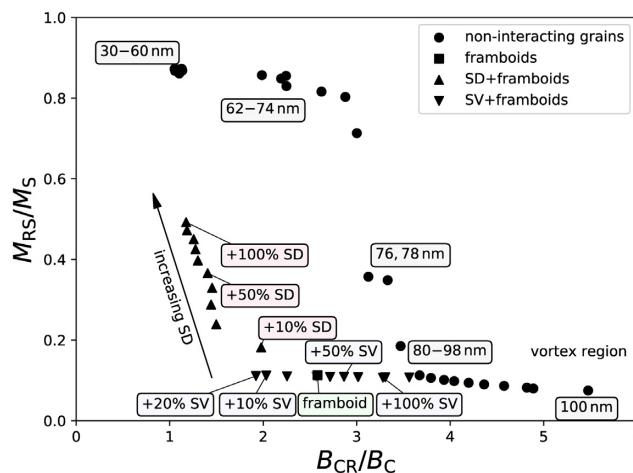


**Figure 7.** Day plot with simulation results for individual grains of different sizes, the frambooid with 30 nm particles, mixtures of frambooids with isolated SD grains (upward-pointing triangles), and isolated SV grains (downward-pointing triangles). The mixtures contain increasing proportions of SD and SV material, ranging from 10 to 100 percent by mass of the frambooid contribution. SD contributions consist of grains in the 30–48 nm size range, and SV grains in the 70–80 nm range. Solutions for isolated particles are from Valdez-Grijalva *et al.* (2018a). All simulations are for distributions of randomly oriented particles.

greigite crystals follow a contrasting trend. This is primarily because the framboidal signal contributes to  $M_S$  but less significantly to  $M_{RS}$ , which gives rise to low  $M_{RS}/M_S$  ratios. Increasing contents of isolated SD or SV particles have contrasting effects on the Day plot: increasing the SD content increases the remanence and decreases  $B_{CR}/B_C$ , whereas, increasing the SV content has little effect on  $M_{RS}/M_S$  while initially decreasing  $B_{CR}/B_C$ , before increasing it. The contrasting data positions for the different particle types and mixtures indicate that other processes also contribute to ambiguity in interpreting data distributions in the Day plot as suggested by Roberts *et al.* (2018a).

## 5 CONCLUSIONS

The FORC response of simulated framboidal greigite ensembles has been calculated with a micromagnetic algorithm. Framboidal greigite clusters that consist of interacting SD particles have similar FORC responses to MD grains. Even though the FORC response has been calculated for framboids that consist of 30 nm SD particles that have stable behaviour when isolated, these observations are likely to hold for framboids composed of larger grains because it is to be expected that such tightly packed particles will produce MD-like FORC signals. Greigite is found to occur commonly with other iron sulphides like pyrite (Rowan & Roberts 2006; Rowan *et al.* 2009), and it is uncommon to find large, MD greigite grains. This means that if a sample is known to contain greigite, MD-like FORC signals could be due to framboidal or other forms of strongly interacting greigite.

## ACKNOWLEDGEMENTS

This research was funded by the Instituto Mexicano del Petróleo (M.A. Valdez-Grijalva), National Science Foundation Grant No. EAR1827263 (L. Nagy), NERC grant NE/J020508/1 (A. R. Muxworthy and W. Williams) and Australian Research Council grant DP160100805 (A. P. Roberts and A. R. Muxworthy). The Terravulf III cluster is supported through the AuScope Australian Geophysical Observing System (AGOS) and the Australian National Collaborative Research Infrastructure Strategy (NCRIS). Model results will be made available on FigShare upon acceptance of this paper.

## REFERENCES

- Ariztegui, D. & Dobson, J., 1996. Magnetic investigations of framboidal greigite formation: a record of anthropogenic environmental changes in eutrophic Lake St. Moritz, Switzerland, *Holocene*, **6**(2), 235–241.
- Brown, W.F., 1963. *Micromagnetics*, Interscience.
- Carvallo, C., Muxworthy, A.R., Dunlop, D.J. & Williams, W., 2003. Micromagnetic modeling of first-order reversal curve (FORC) diagrams for single-domain and pseudo-single-domain magnetite, *Earth Planet. Sci. Lett.*, **213**(3), 375–390.
- Chang, L., Roberts, A.P., Tang, Y., Rainford, B.D., Muxworthy, A.R. & Chen, Q., 2008. Fundamental magnetic parameters from pure synthetic greigite ( $\text{Fe}_3\text{S}_4$ ), *J. geophys. Res.*, **113**(B6), doi:10.1029/2007JB005502.
- Chou, Y.M., Song, S.R., Aubourg, C., Song, Y.F., Boullier, A.M., Lee, T.Q., Evans, M., Yeh, E.C. & Chen, Y.M., 2012. Pyrite alteration and neoformed magnetic minerals in the fault zone of the Chi-Chi earthquake ( $M_w$  7.6, 1999): evidence for frictional heating and co-seismic fluids, *Geochem. Geophys. Geosyst.*, **13**(8), doi:10.1029/2012GC004120.
- Day, R., Fuller, M. & Schmidt, V.A., 1977. Hysteresis properties of titanomagnetites: grain-size and compositional dependence, *Phys. Earth Planet. Inter.*, **13**(4), 260–267.
- Dumas, R.K., Li, C.P., Roshchin, I.V., Schuller, I.K. & Liu, K., 2007. Magnetic fingerprints of sub-100 nm Fe dots, *Phys. Rev. B*, **75**(13), 134405.
- Ebert, Y., Shaar, R., Emmanuel, S., Nowaczyk, N. & Stein, M., 2018. Overwriting of sedimentary magnetism by bacterially mediated mineral alteration, *Geology*, **46**(4), 291–294.
- Egli, R., 2013. VARIFORC: An optimized protocol for calculating non-regular first-order reversal curve (FORC) diagrams, *Global Planet. Change*, **110**, 302–320.
- Egli, R. & Winklhofer, M., 2014. Recent developments on processing and interpretation aspects of first-order reversal curves (FORC), *Proc. Kazan Univ. Nat. Sci.*, **156**(1), 14–53.
- Emmerton, S., Muxworthy, A.R., Sephton, M.A., Aldana, M., Costanzo-Alvarez, V., Bayona, G. & Williams, W., 2013. Correlating biodegradation to magnetization in oil bearing sedimentary rocks, *Geochim. Cosmochim. Acta*, **112**, 146–165.
- Fredkin, D.R. & Koehler, T.R., 1990. Hybrid method for computing demagnetizing fields, *IEEE Trans. Magn.*, **26**(2), 415–417.
- Harrison, R.J. & Feinberg, J.M., 2008. FORCinel: an improved algorithm for calculating first-order reversal curve distributions using locally weighted regression smoothing, *Geochem. Geophys. Geosyst.*, **9**(5), doi:10.1029/2008GC001987.
- Harrison, R.J., Dunin-Borkowski, R.E. & Putnis, A., 2002. Direct imaging of nanoscale magnetic interactions in minerals, *Proc. Natl. Acad. Sci. USA*, **99**(26), 16556–16561.
- Hubert, A. & Schäfer, R., 2000. *Magnetic Domains: The Analysis of Magnetic Microstructures*, Springer.
- Hüsing, S.K., Dekkers, M.J., Franke, C. & Krijgsman, W., 2009. The Tortonian reference section at Monte dei Corvi (Italy): evidence for early remanence acquisition in greigite-bearing sediments, *Geophys. J. Int.*, **179**(1), 125–143.
- Landau, L.D. & Lifshitz, E., 1935. On the theory of the dispersion of magnetic permeability in ferromagnetic bodies, *Phys. Z. Sowjetunion*, **8**(153), 101–114.
- Li, G. *et al.*, 2014. High-purity  $\text{Fe}_3\text{S}_4$  greigite microcrystals for magnetic and electrochemical performance, *Chem. Mater.*, **26**(20), 5821–5829.
- Muxworthy, A.R. & Dunlop, D.J., 2002. First-order reversal curve (FORC) diagrams for pseudo-single-domain magnetites at high temperature, *Earth Planet. Sci. Lett.*, **203**(1), 369–382.
- Muxworthy, A.R., Williams, W. & Virdee, D., 2003. Effect of magnetostatic interactions on the hysteresis parameters of single-domain and pseudo-single-domain grains, *J. geophys. Res.*, **108**(B11), doi:10.1029/2003JB002588.
- Muxworthy, A.R., Heslop, D. & Williams, W., 2004. Influence of magnetostatic interactions on first-order-reversal-curve (FORC) diagrams: a micromagnetic approach, *Geophys. J. Int.*, **158**(3), 888–897.
- Muxworthy, A.R., Williams, W., Roberts, A.P., Winklhofer, M., Chang, L. & Pósfai, M., 2013. Critical single domain grain sizes in chains of interacting greigite particles: implications for magnetosome crystals, *Geochem. Geophys. Geosyst.*, **14**(2), 5430–5441.
- Ó Conbhuí, P., Williams, W., Fabian, K., Ridley, P., Nagy, L. & Muxworthy, A.R., 2018. MERRILL: micromagnetic Earth Related Robust Interpreted Language Laboratory, *Geochem. Geophys. Geosyst.*, **19**, 1080–1106.
- Ohfuji, H. & Rickard, D., 2005. Experimental syntheses of framboids—a review, *Earth-Sci. Rev.*, **71**(3), 147–170.
- Ohfuji, H., Rickard, D., Light, M.E. & Hursthouse, M.B., 2006. Structure of framboidal pyrite: a single crystal X-ray diffraction study, *Eur. J. Min.*, **18**(1), 93–98.
- Pike, C. & Fernandez, A., 1999. An investigation of magnetic reversal in submicron-scale Co dots using first order reversal curve diagrams, *J. Appl. Phys.*, **85**(9), 6668–6676.
- Pike, C.R., Roberts, A.P. & Verosub, K.L., 1999. Characterizing interactions in fine magnetic particle systems using first order reversal curves, *J. Appl. Phys.*, **85**(9), 6660–6667.
- Pike, C.R., Roberts, A.P., Dekkers, M.J. & Verosub, K.L., 2001. An investigation of multi-domain hysteresis mechanisms using FORC diagrams, *Phys. Earth Planet. Inter.*, **126**(1), 11–25.

- Rickard, D., 2019. Sedimentary pyrite framboid size-frequency distributions: a meta-analysis, *Palaeogeogr. Palaeoclimatol. Palaeoecol.*, **522**, 62–75.
- Roberts, A.P., 2015. Magnetic mineral diagenesis, *Earth-Sci. Rev.*, **151**, 1–47.
- Roberts, A.P., Pike, C.R. & Verosub, K.L., 2000. First-order reversal curve diagrams: a new tool for characterizing the magnetic properties of natural samples, *J. geophys. Res.*, **105**(B12), 28 461–28 475.
- Roberts, A.P., Chang, L., Rowan, C.J., Horng, C.S. & Florindo, F., 2011. Magnetic properties of sedimentary greigite (Fe<sub>3</sub>S<sub>4</sub>): an update, *Rev. Geophys.*, **49**(1), doi:10.1029/2010RG000336.
- Roberts, A.P., Heslop, D., Zhao, X. & Pike, C.R., 2014. Understanding fine magnetic particle systems through use of first-order reversal curve diagrams, *Rev. Geophys.*, **52**(4), 557–602.
- Roberts, A.P., Tauxe, L., Heslop, D., Zhao, X. & Jiang, Z., 2018a. A critical appraisal of the Day diagram, *J. geophys. Res.*, **123**(4), 2618–2644.
- Roberts, A.P. et al., 2018b. Signatures of reductive magnetic mineral diagenesis from unmixing of first-order reversal curves, *J. geophys. Res.*, **123**(6), 4500–4522.
- Rowan, C.J. & Roberts, A.P., 2006. Magnetite dissolution, diachronous greigite formation, and secondary magnetizations from pyrite oxidation: unravelling complex magnetizations in Neogene marine sediments from New Zealand, *Earth Planet. Sci. Lett.*, **241**(1), 119–137.
- Rowan, C.J., Roberts, A.P. & Broadbent, T., 2009. Reductive diagenesis, magnetite dissolution, greigite growth and paleomagnetic smoothing in marine sediments: a new view, *Earth Planet. Sci. Lett.*, **277**(1), 223–235.
- Snowball, I.F., 1997. Gyromagnetic magnetization and the magnetic properties of greigite-bearing clays in southern Sweden, *Geophys. J. Int.*, **129**(3), 624–636.
- Valdez-Grijalva, M.A. & Muxworthy, A.R., 2019. First-order reversal curve (FORC) diagrams of nanomagnets with cubic magnetocrystalline anisotropy, *J. Magn. Magn. Mater.*, **471**, 359–364.
- Valdez-Grijalva, M.A., Muxworthy, A.R., Williams, W., Ó Conbhuí, P., Nagy, L., Roberts, A.P. & Heslop, D., 2018a. Magnetic vortex effects on first-order reversal curve (FORC) diagrams for greigite dispersions, *Earth Planet. Sci. Lett.*, **501**, 103–111.
- Valdez-Grijalva, M.A., Nagy, L., Muxworthy, A.R., Williams, W. & Fabian, K., 2018b. The magnetic structure and palaeomagnetic recording fidelity of sub-micron greigite (Fe<sub>3</sub>S<sub>4</sub>), *Earth Planet. Sci. Lett.*, **483**, 76–89.
- Winklhofer, M., Chang, L. & Eder, S. H.K., 2014. On the magnetocrystalline anisotropy of greigite (Fe<sub>3</sub>S<sub>4</sub>), *Geochem. Geophys. Geosyst.*, **15**(4), 1558–1579.
- Zhao, X., Roberts, A.P., Heslop, D., Paterson, G.A., Li, Y. & Li, J., 2017. Magnetic domain state diagnosis using hysteresis reversal curves, *J. geophys. Res.*, **122**(7), 4767–4789.

## SUPPORTING INFORMATION

Supplementary data are available at [GJI](https://doi.org/10.1111/gji.12222) online.

**ESM\_1.m4v, ESM\_2.m4v, ESM\_3.m4v, ESM\_4.m4v, ESM\_5.m4v, valdez\_et al\_2019\_SM.pdf**

Please note: Oxford University Press is not responsible for the content or functionality of any supporting materials supplied by the authors. Any queries (other than missing material) should be directed to the corresponding author for the paper.